Short and intermediate range order in amorphous $GeSe_2$

Carlo Massobrio[1] and Alfredo Pasquarello[2,3]
[1]*Institut de Physique et de Chimie des Matériaux de Strasbourg, 23 rue du Loess, Boîte Postale 43, F-67034 Strasbourg Cedex 2, France*
[2]*Ecole Polytechnique Fédérale de Lausanne (EPFL), Institute of Theoretical Physics, CH-1015 Lausanne, Switzerland*
[3]*Institut Romand de Recherche Numérique en Physique des Matériaux (IRRMA), CH-1015 Lausanne, Switzerland*
(Received 28 January 2008; revised manuscript received 26 March 2008; published 17 April 2008)

By using first-principle molecular dynamics within density functional theory, we study the structural properties of amorphous $GeSe_2$ at a temperature T of 300 K. For each property, a statistical average is obtained from six independent partial averages taken on temporal trajectories, each one lasting 12 ps. Each trajectory stems from an initial configuration of the liquid phase at $T=1100$ K and is generated by extensive annealing at $T=300$ K. Overall, our level of theory provides a picture of this prototypical disordered network-forming glass that is quantitatively consistent with neutron diffraction data. Very satisfactory agreement with experiments is obtained for the pair correlation functions $g_{GeSe}(r)$ and $g_{SeSe}(r)$ in terms of peak intensities and positions. This holds true also for the amount of Se-Se homopolar bonds and the Ge-Se and Se-Se coordination numbers. Conversely, the $g_{GeGe}(r)$ pair correlation function is much less structured around the main peak position and the concentration of Ge-Ge homopolar bonds is lower than in the experiment. The network organizes itself through the predominant presence of $GeSe_4$ tetrahedra. However, other coordinations occur in non-negligible proportions for both Ge and Se. Total and partial structure factors reproduce very well the experimental patterns for wave numbers k larger than 2 $Å^{-1}$. For smaller k values, the largest difference between theory and experiment is exhibited by the $S_{GeGe}(k)$ structure factor, showing a FSDP of lower intensity in the simulation. In agreement with experimental results, a sizeable feature is found at the FSDP location in the Bhatia–Thornton concentration-concentration structure factor $S_{CC}(k)$.

DOI: 10.1103/PhysRevB.77.144207 PACS number(s): 61.25.Em, 61.20.Ja, 71.15.Pd

I. INTRODUCTION

One of the most debated issues in glass science is the origin and the extent of chemical disorder in disordered networks.[1] In the case of AX_2 systems, a departure from chemical order arises from the presence of homopolar bonds and coordinations deviating from that of the main constitutive unit, the AX_4 tetrahedron.[2] In terms of the views proposed to describe the structure of glasses, a network characterized by broken chemical order (BCO) contrasts the chemically ordered continuous random network (CORN), in which the number of heterogeneous bonds is maximized.[3] Networks exhibiting either one of these two behaviors can be found within the AX_2 (i.e., $A_{1-n}X_n$, $n=1/3$) family of glasses ($A=Si,Ge$; $X=O,S,Se$). A well known example of CORN is amorphous SiO_2, which is constituted of undefective corner-sharing tetrahedra.[4–6] The occurrence of a departure from chemical order in $GeSe_2$ has been long-time controversial until the BCO nature of $GeSe_2$ (a-$GeSe_2$) was unraveled by measurements that gave clearcut evidence of the presence of homopolar bonds.[7–10] Signatures of the BCO nature of $GeSe_2$ were first found via Raman, Mössbauer, and scanning calorimetry experiments performed on a variety of concentrations close to $n=1/3$ in $Ge_{1-n}Se_n$ systems.[7,8] Later, percentages of Ge and Se homopolar bonds were obtained through the full set of partial structure factors and pair distribution functions, which are measured by using the method of isotopic substitution in neutron diffraction.[9,10] These sets of data superseded early indications pointing to the CORN nature of a-$GeSe_2$.[11–13]

In a-$GeSe_2$, the occurrence of broken chemical order does not prevent the establishment of intermediate range order. This degree of structural organization involves distances much longer than nearest-neighbor bonds and manifests itself through the appearance of the first sharp diffraction peak (FSDP) in the total neutron structure factor.[14] The coexistence between a departure from chemical order at short range and the persistence of intermediate range order is an elusive feature in a-$GeSe_2$, which calls for a precise understanding of its structure at the atomic scale. In this context, several molecular dynamics models of a-$GeSe_2$ have been devised. The effective two- and three-body potentials constructed by Vashishta and co-workers[15] provided a first, satisfactory interpretation of the total neutron diffraction data but were unable to predict miscoordinations and homopolar bonds. The use of an approximate density functional (DFT) framework, which was based on a non-self-consistent electronic structure scheme, the local density approximation of DFT, and a minimal basis set, yielded an improved description of these aspects.[16–19] Some of these calculations were carried out in conjunction with a set of optimization techniques, in which experimental information and constraints on the coordinations of specific subunits were introduced.[20–22] Very recently, interatomic potentials derived from first-principles calculations have also been proposed.[23] However, homopolar Ge-Ge bonds were absent within this description.

In this paper, we study the structural properties of a-$GeSe_2$ via first-principles molecular dynamics in the framework of density functional theory. We focus on the pair correlation functions $g_{\alpha\beta}(r)$, the partial structure factors $S_{\alpha\beta}(k)$, the bond angle distribution, and a neighbor analysis based on a ring statistics. We take statistical averages over trajectories produced by quenching atomic configurations of the liquid and allowing for significant structural relaxation,

so as to minimize the memory of the starting configurations. We perform a detailed comparison between our theory and the neutron diffraction data that are obtained by Salmon and co-workers,[9,10] highlighting the good agreement and identifying the remaining differences. An account of the structural and vibrational properties of a-$GeSe_2$ based on a single model configuration at $T=0$ K is given elsewhere.[24]

This paper is organized as follows. In Sec. II, we describe how we generated our model structures of a-$GeSe_2$. Our results are collected in two sections, which are devoted to real space properties (Sec. III) and reciprocal space properties (Sec. IV). Conclusive remarks can be found in Sec. V.

II. THEORETICAL MODEL

We simulated a system of 40 Ge and 80 Se at constant volume. A periodically repeated cubic cell of size 15.16 Å was adopted, corresponding to an experimental density of 0.034 $Å^{-3}$ at $T=300$ K.[25] This system size is sufficiently large to cover the region of wave vectors in which the FSDP appears. The smallest wave vector compatible with our supercell is $k_{min}=0.4$ $Å^{-1}$, significantly smaller than the FSDP wave vector $k_{FSDP}=\sim 1$ $Å^{-1}$ (Ref. 9). The region of wave vectors, in which the FSDP appears is described by as much as seven discrete wave vectors compatible with the periodicity of our supercell. A more detailed rationale of our choice of system size has been developed in previous papers.[26–29] In particular, we refer to the analyses developed in Ref. 28 on the range of real space correlations that are responsible for the appearance of the FSDP. The electronic structure was described within density functional theory and evolved self-consistently during the motion.[30,31] Valence electrons were treated explicitly, in conjunction with normconserving pseudopotentials to account for core-valence interactions. We resorted to the Perdew–Wang generalized gradient approximation detailed in Ref. 32, with normconserving pseudopotentials generated as in Ref. 33. The wave functions are expanded at the Γ point of the supercell. The energy cutoff is taken equal to $E_c=20$ Ry. We refer to previous studies on liquid $GeSe_2$ for the account of test calculations validating our simulation scheme.[28,34]

To construct our amorphous structure and achieve optimal statistical sampling, we selected six ($N_{st}=6$) configurations separated by 3 ps along a trajectory of 20 ps that was generated previously for the liquid.[28] The corresponding coordinates were rescaled to match the density of the glass and the six subtrajectories were followed in time. For each one of them, the system was cooled from 1100 to 600 K in 22 ps (10 ps at 1100 K, 7 ps at 900 K, and 5 ps at 600 K) and further annealed for 22 ps at $T=300$ K. First-principles molecular dynamics were performed by using Nosé–Hoover thermostats at the given target temperature.[35,36] The interval of 22 ps in between 1100 and 600 K allowed for significant atomic diffusion after the density change. The second interval of the same length (22 ps at $T=300$ K) had the purpose to fully relax the amorphous structure. This is exemplified by comparing the pair correlation functions $g^{th}_{\alpha\beta}(r)$ averaged over the first 5 ps $[g^{th\text{-}a}_{\alpha\beta}(r)]$ and over the last 12 ps $[g^{th\text{-}b}_{\alpha\beta}(r)]$ of this interval for a single subtrajectory at $T=300$ K. In Fig. 1, both $g^{th\text{-}a}_{\alpha\beta}(r)$ and $g^{th\text{-}b}_{\alpha\beta}(r)$ are compared to the pair correlation functions $g^{th\text{-}liq}_{\alpha\beta}(r)$ of the liquid.[28] Clearly, the $g^{th\text{-}a}_{\alpha\beta}(r)$ differ from the corresponding $g^{th\text{-}liq}_{\alpha\beta}(r)$ only in the intensities of the peaks and in the depths of the minima. In particular, $g^{th\text{-}a}_{GeGe}(r)$ and $g^{th\text{-}liq}_{GeGe}(r)$ have similar profiles for the whole range of distances. Marked differences appear between $g^{th\text{-}b}_{GeGe}(r)$ and $g^{th\text{-}liq}_{GeGe}(r)$ for $r>4$ Å, with new features that become distinguishable in the $2<r<3.5$ Å range. For $g^{th\text{-}b}_{GeSe}(r)$ and $g^{th\text{-}b}_{SeSe}(r)$, the relaxation led to less significant modifications of the heights of the peaks and the depths of the minima. It is interesting to note that pair correlation functions very close to $g^{th\text{-}a}_{\alpha\beta}(r)$ were obtained through a different quenching schedule. One of the six initial configurations of the liquid state was cooled from 1100 to 300 K, while the density was varied linearly with temperature between those of the liquid and the glass. The thermostat temperature was reduced by 200 K every 8 ps, and a trajectory of 4 ps at $T=300$ K was used to collect the average results. At each variation of the temperature, the atomic coordinates were rescaled to match the appropriate density.

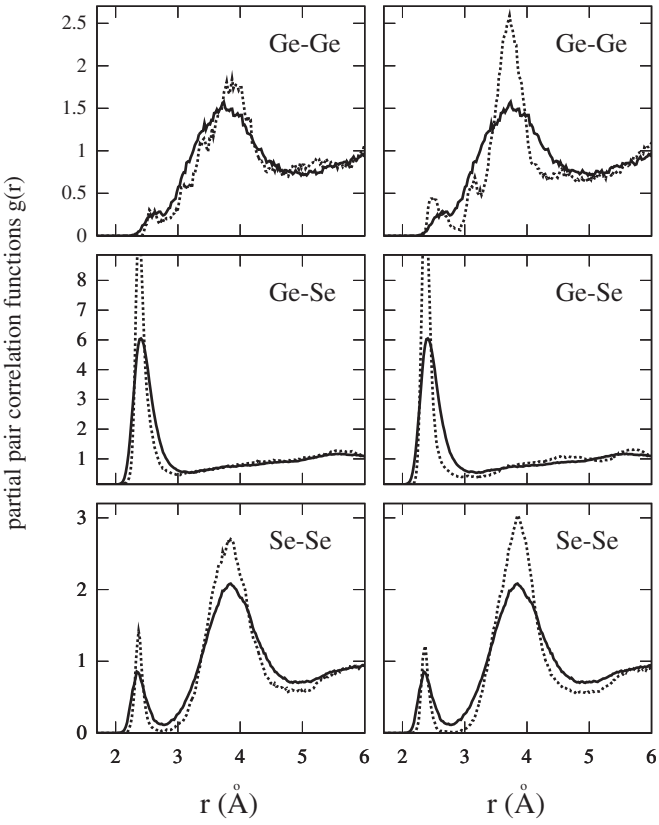

FIG. 1. Pair correlation functions of amorphous $GeSe_2$ (dashed line) at $T=300$ K. On the left: average values $g^{th\text{-}a}_{GeGe}(r)$, $g^{th\text{-}a}_{GeSe}(r)$, and $g^{th\text{-}a}_{SeSe}(r)$ obtained for the first 5 ps of annealing at $T=300$ K compared with the results for the equilibrated liquid (full line, Ref. 28). On the right: average values $g^{th\text{-}b}_{GeGe}(r)$, $g^{th\text{-}b}_{GeSe}(r)$ and $g^{th\text{-}b}_{SeSe}(r)$ obtained for the last 12 ps of annealing at $T=300$ K compared to the results for the equilibrated liquid (full line, Ref. 28). In both cases, the averages are taken on a single temporal trajectory.

The average results that are presented in this work have been obtained as follows. We first took statistical averages over the last 12 ps for each single subtrajectory at T

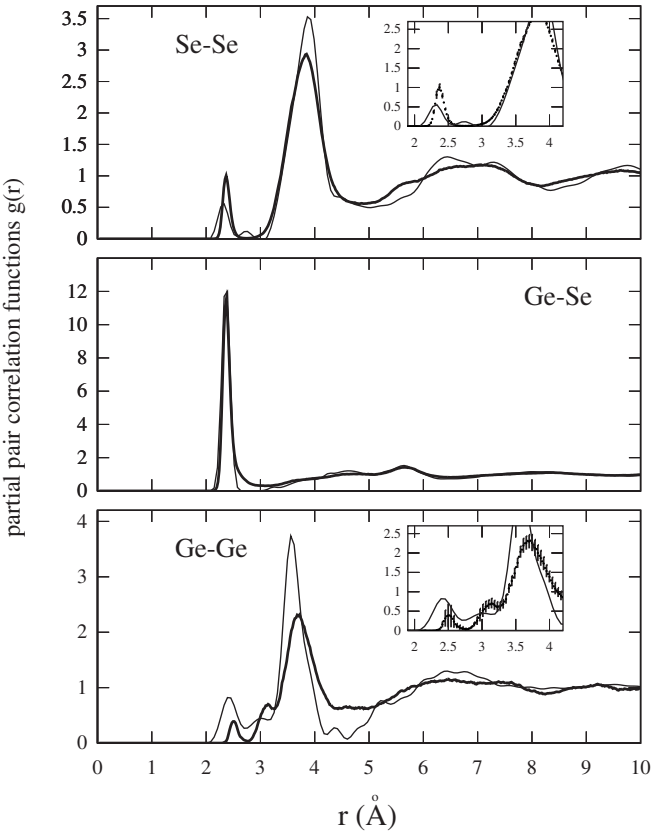

FIG. 2. Pair correlation functions of amorphous $GeSe_2$: present simulation (thick line) compared to the experimental data of Ref. 9 (thin line). In the case of $g_{GeGe}(r)$ and $g_{SeSe}(r)$, the interval of distances between 1.9 and 4.2 Å has been magnified in the inset and the associated error bars are shown.

=300 K. Then, from this set of N_{st} partial averages, we extracted global averages (mean values). For each subtrajectory, typical standard deviations correspond to only 0.5% of the partial average. This is due to the limited thermal fluctuations of the instantaneous quantities at $T=300$ K. In order to reflect the variations found among the whole population of six partial averages, we expressed the statistical errors of the mean values σ_{mean} as $\sigma/\sqrt{N_{st}-1}$, where σ is half the largest difference among the N_{st} partial averages.

III. REAL SPACE PROPERTIES

A. Pair correlation functions

In Fig. 2, we display calculated and experimental partial pair correlation functions (PCFs) $g^{th}_{\alpha\beta}(r)$. Peak positions and coordination numbers $n_{\alpha\beta}$ are reported in Table I, where they are compared to experimental data of Ref. 10. In the case of $g_{SeSe}(r)$, our calculations reproduce well the shape of the experimental pair correlation function. The presence of homopolar Se-Se bonds is reflected by the first peak, which is located at a value of r 2% larger than in $g^{exp}_{SeSe}(r)$. In our calculation this peak has a higher intensity, leading to the overestimation of n_{SeSe} (0.27 ± 0.03 against 0.2). Statistical errors in the range of distances around the first peak are as

TABLE I. First (FP), second (SP), and third (TP) peak positions in the experimental (Ref. 10) and theoretical $g_{\alpha\beta}(r)$. $n_{\alpha\beta}$, $n'_{\alpha\beta}$ and $n''_{\alpha\beta}$ are the corresponding coordination numbers. IR corresponds to the integration range for each coordination number. In our calculations the IRs are taken as the intervals between the two minima preceding and following a maximum, respectively. Note that we had no signature of a second peak in $g^{th}_{SeSe}(r)$. For clarity, peak position, integration range, and coordination number relative to the second peak in $g^{th}_{SeSe}(r)$ have been compared to the corresponding values relative to the third peak in the experimental $g^{exp}_{SeSe}(r)$.

$g_{\alpha\beta}(r)$	FP (Å)	$n_{\alpha\beta}$	IR[FP] (Å)
$g^{exp}_{GeGe}(r)$	2.42	0.25	0–2.73
$g^{th}_{GeGe}(r)$	2.50 ± 0.03	0.07 ± 0.04	0–2.75
$g^{exp}_{GeSe}(r)$	2.36	3.71	2.09–2.61
$g^{th}_{GeSe}(r)$	2.37 ± 0.01	3.86 ± 0.08	2.07–3.09
$g^{exp}_{SeSe}(r)$	2.32	0.20	0–2.55
$g^{th}_{SeSe}(r)$	2.37 ± 0.01	0.27 ± 0.03	0–2.73
	SP (Å)	$n'_{\alpha\beta}$	IR[SP] (Å)
$g^{exp}_{GeGe}(r)$	3.02	0.34	2.73–3.19
$g^{th}_{GeGe}(r)$	3.14 ± 0.04	0.30 ± 0.06	2.75–3.27
$g^{exp}_{SeSe}(r)$	2.74	0.06	2.55–3.09
	TP (Å)	$n''_{\alpha\beta}$	IR[TP] (Å)
$g^{exp}_{GeGe}(r)$	3.57	3.2	3.19–4.23
$g^{th}_{GeGe}(r)$	3.72 ± 0.01	3.31 ± 0.05	3.27–4.43
$g^{exp}_{SeSe}(r)$	3.89	9.3	3.09–4.39
$g^{th}_{SeSe}(r)$	3.84 ± 0.02	10.50 ± 0.10	2.73–4.50

large as 10% due to the occurrence of different distributions of Se_n chains in the subtrajectories. On the average, homopolar connections lead to eight Se dimers plus one Se trimer. We found no sign of a second, small peak for $r<3$ Å, as reported in Ref. 10. The positions of the main peak (termed third peak in Table I) in $g^{th}_{SeSe}(r)$ and $g^{exp}_{SeSe}(r)$ differ by only 2%, but the intensity in $g^{th}_{SeSe}(r)$ is lower by 17%. For $r>5$ Å, $g^{exp}_{SeSe}(r)$ is more structured than $g^{th}_{SeSe}(r)$, with a minimum of larger and deeper width in the interval $5<r<6$ Å.

The pair correlation functions $g^{exp}_{GeSe}(r)$ and $g^{th}_{GeSe}(r)$ are very close in terms of the position, the intensity, and the width of the main peak (Fig. 2). The only notable difference is a sharper decay to zero of $g^{exp}_{GeSe}(r)$ for $r>2.5$ Å. This results in a higher theoretical n_{GeSe} (3.86 against 3.71, Ref. 10), which is both consistent with a departure from chemical order ($n_{GeSe}=4$).

The comparison between $g^{th}_{GeGe}(r)$ and $g^{exp}_{GeGe}(r)$ reveals in both PCFs three distinct features in the region $2<r<4$ Å. The first and third features show up as distinct peaks, while the second feature is discernible as a shoulder. These features can be associated to homopolar Ge-Ge bonds, Ge atoms involved in edge-sharing connections, and Ge atoms involved in corner-sharing connections, respectively. The error bars amount to as much as 50% in the interval $2.3<r<2.7$ Å,

TABLE II. Average number $n_\alpha(l)$ (expressed as a percentage) of Ge and Se atoms l-fold coordinated at a distance of 2.7 Å. For each value of $n_\alpha(l)$, we give the identity and the number of the Ge and Se neighbors. For instance, $GeSe_3$ with $l=4$ means a fourfold coordinated Ge with one Ge and three Se nearest-neighbors. We also compare calculated and experimental values (in percentage) for the number of Ge atoms forming edge-sharing connections, $N_{Ge}(ES)$, the number of Ge atoms forming corner-sharing connections, $N_{Ge}(CS)$, the number of Ge atoms involved in homopolar bonds, $N_{Ge\text{-}Ge}$, and the number of Se atoms involved in homopolar bonds, $N_{Se\text{-}Se}$. Experimental values are taken from Ref. 10.

Ge	$l=1$		$l=2$	
	Se	5 ± 1	Se_2	12 ± 1
	$l=3$		$l=4$	
	Se_3	8 ± 1	$GeSe_3$	5 ± 2
			Se_4	70 ± 4
Se	$l=1$		$l=2$	
	Ge	4 ± 1	Se_2	3 ± 1
			SeGe	21 ± 1
			Ge_2	69 ± 1
	$l=3$			
	Ge_3	4 ± 1		
	$N_{Ge}(ES)$	$N_{Ge}(CS)$	$N_{Ge\text{-}Ge}$	$N_{Se\text{-}Se}$
This work	45 ± 4	50 ± 6	5 ± 2	24 ± 2
Expt.	34	41	25	20

which includes the first peak of $g^{th}_{GeGe}(r)$. A less structured shape of $g^{th}_{GeGe}(r)$ when compared to $g^{exp}_{GeGe}(r)$, together with longer interatomic Ge-Ge distances, were also found in previous simulations of liquid $GeSe_2$ and liquid GeSe.[28,37] These shortcomings are a consequence of current limitations in our description of Ge-Ge correlations within the Perdew–Wang generalized gradient approximation of DFT. It has been previously suggested that residual differences between theory and experiments could be attributed to an insufficient account of the ionic character of these systems.[28,37] This would be consistent with our findings of excessively large Ge-Ge bond lengths, characteristic of metallic liquid Ge. The calculated n_{GeGe} (0.07 ± 0.04) is much smaller than the experimental value of 0.25.[9,10] Large error bars on n_{GeGe} are due to the absence of any Ge-Ge homopolar bond in two of the six subtrajectories, at variance with the presence of one, two, and four Ge-Ge homopolar bonds in the other four subtrajectories. Reducing the dispersion at nearest-neighbor distances in $g^{th}_{GeGe}(r)$, and to a lesser extent in $g^{th}_{SeSe}(r)$, would require further extending the statistical sampling.

B. Coordination numbers

Information on the short range structure of a-$GeSe_2$ is given in Table II. We defined $n_\alpha(l)$ the average number of atoms of species αl-fold coordinated within a cutoff radius of 2.7 Å, where α are Ge or Se atoms. The cutoff radius was chosen to include in the coordination shell of Ge only Ge-Ge contacts, forming true homopolar bonds. This amounts to exclude pairs of Ge atoms facing each other within fourfold rings in edge-sharing connections [see $g^{th}_{GeGe}(r)$ in Fig. 2], typically at distances close to 3 Å. The number of fourfold coordinated Ge atoms and of twofold coordinated Se atoms is higher than in the liquid [$(75\pm6)\%$ vs 61% and $(93\pm6)\%$ vs 70%, respectively], indicating that the chemical order is partially restored upon cooling. In addition to the largely predominant tetrahedral arrangement, the Ge atoms also show first-neighbor shells composed of GeSe, $GeSe_2$, and $GeSe_3$. All of the homopolar Ge connections involve pairing of two Ge-Se_3 units to form a Se_3-Ge-Ge-Se_3 ethanelike group. There are $N_{Ge\text{-}Ge}=(5\pm2)\%$ of Ge atoms involved in homopolar bonds. In the case of Se, $(21\pm1)\%$ of Se atoms are twofold coordinated with one Se and one Ge atom in the first-neighbor shell. These correspond to Se_2 dimers, while the signature of Se_3 trimers is given by the $(3\pm1)\%$ of Se atoms twofold connected to a pair of Se atoms. There are $N_{Se\text{-}Se}=(24\pm2)\%$ of Se atoms involved in homopolar bonds.

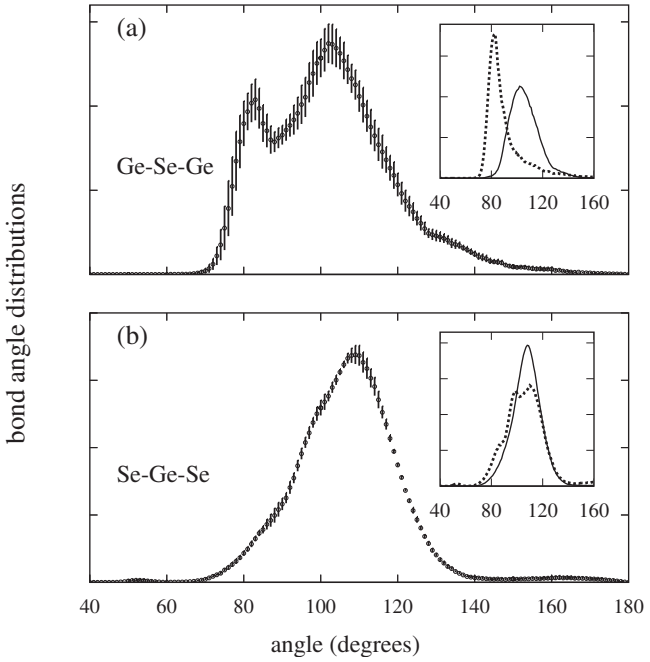

FIG. 3. Bond-angle distributions of amorphous $GeSe_2$: (a) Ge-Se-Ge and (b) Se-Ge-Se. In the inset of panel (a), the decomposition of the Ge-Se-Ge distribution distinguishes the cases in which the two Ge atoms of the Ge-Se-Ge triad are involved in an edge-sharing connection (dashed) or not (solid). In the inset of panel (b), the decomposition of the Se-Ge-Se distribution distinguishes the cases in which the Ge atom of the Se-Ge-Se triads is involved in an edge-sharing configuration (dashed) or not (solid).

C. Bond angle distributions

In Fig. 3, we show the distribution of the Se-Ge-Se (θ_{SeGeSe}) and Ge-Se-Ge (θ_{GeSeGe}) bond angles. These distributions have been calculated by including neighbors separated by less than 3 Å. The Ge-Se-Ge bond distribution is characterized by two main peaks at 83° and 102°. These results agree well with the experimental estimates of 80° and 98° provided by Salmon.[38] The first peak arises from edge-

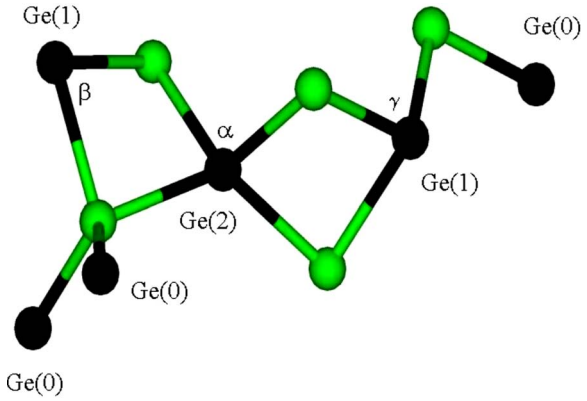

FIG. 4. (Color online) Three-dimensional view of structural subunits of amorphous $GeSe_2$ high-lighting different Se-Ge-Se triads and their corresponding θ_{SeGeSe} angles: α, β, and γ. Ge atoms are dark (black) and Se atoms are light (green). Bonds are drawn when two atoms are separated by less than 3 Å, the first minimum in the Ge-Se radial pair distribution function. Ge(0), Ge(1), and Ge(2) are Ge atoms involved in 0, 1, and 2 fourfold rings, respectively.

sharing tetrahedra, i.e., Ge-centered subunits, which have in common two Se atoms. These subunits give rise to fourfold rings. The main peak then results from corner-sharing tetrahedra, which share only a single Se atom. This interpretation is confirmed by the decomposition of the Ge-Se-Ge bond angle distribution in the inset of Fig. 3(a), in which the contribution of Ge-Se-Ge triads resulting from edge-sharing connections is distinguished.

The maximum of θ_{SeGeSe} lies at 109° due to the predominant tetrahedral nature of the network. However, the Se-Ge-Se bond angle distribution is not symmetric showing a broadening in the interval of 80°–100°. To analyze the origins of this feature, we decomposed θ_{SeGeSe} distinguishing the contribution of Ge atoms either involved or not involved in edge-sharing connections [see inset in Fig. 3(b)]. The distribution associated to Ge atoms not involved in edge-sharing connections has a symmetric bell shape around the maximum at 109°, as expected for a bond angle within a corner-sharing tetrahedron. The distribution resulting from Ge atoms in edge-sharing connections shows a more complex structure, including a shoulder and two peaks. The shoulder in the interval between 80° and 90° is attributed to Se-Ge-Se angles involving Se atoms on two different and yet connected fourfold rings, having in common a Ge atom (angle α in Fig. 4). The first peak at 98°, on the left, is associated with Se-Ge-Se triads, entirely belonging to a fourfold ring (angle β in Fig. 4). Finally, the second peak, on the right, located at 110°, reflects Se-Ge-Se triads in which at least one of the Se atoms does not belong to a fourfold ring, being involved in a corner-sharing connection (angle γ in Fig. 4).

D. Ring statistics

Our distribution of rings is given in Table III. We used the counting algorithm based on the shortest-path criterion first proposed by King and then improved by Franzblau.[39–41] Cutoff radii were taken equal to 2.7 Å for Ge-Ge interactions and to 3.0 Å for Ge-Se and Se-Se interactions. Even-membered rings are more numerous than odd-membered ones, in particular, for ring sizes up to 12 atoms, none of the odd-membered ring sizes occurs more frequently than any of the even-membered ones. Due to the larger number of Se-Se homopolar bonds, a preference for Se-rich rings is observed in odd-membered rings. Fourfold and sixfold rings are largely predominant and mostly characterized by an equal number of Ge and Se atoms, with a very few Se-rich configurations.

Our statistics also provide the number of Ge atoms that belong to zero, one, and two fourfold rings. These Ge atoms are termed Ge(0), Ge(1), and Ge(2) (see Fig. 4). We derived that $(55\pm2)\%$ of the Ge atoms do not belong to fourfold rings, $(40\pm3)\%$ belong to a single fourfold ring, and $(5\pm1)\%$ belong to two fourfold rings. By summing up Ge(1) and Ge(2), one obtains the number of Ge atoms in edge-sharing configurations, $N_{Ge}^{th(a)}(ES)=(45\pm4)\%$. This value could be compared to the experimental estimate of $N_{Ge}^{exp}(ES)=34\%$ derived in Ref. 10 through the integration of $g_{GeGe}^{exp}(r)$ around the second peak at 3.02 Å (see Table I). However, it should be noted that application of the latter procedure to our model yields $N_{Ge}^{th(b)}(ES)=(30\pm6)\%$, corresponding to an integration between the two minima at $r_{min1}=2.75$ Å and $r_{min2}=3.27$ Å. The comparison between $N_{Ge}^{th(a)}(ES)$ and $N_{Ge}^{th(b)}(ES)$ indicates that the integration procedure underestimates the number of edge-sharing configurations. Indeed, it misses all edge-sharing connections, in which the Ge atoms are separated by more than r_{min2}.

TABLE III. Distribution of rings in amorphous $GeSe_2$. NR is the total number of rings of a given size. NR (n Ge) is the number of rings having n Ge atoms ($n=1,\ldots,6$ Ge). Statistical errors do not exceed 10% for rings of size smaller than 5 and attain 20% for larger sizes.

Ring size	3	4	5	6	7	8	9	10	11	12
NR	0.7	10.3	2.4	9.9	2.0	4.2	1.5	2.8	1.7	4.3
NR(1 Ge)	0.7	0.1								
NR(2 Ge)		10.2	2.1	0.4						
NR(3 Ge)			0.3	9.5	2.0	0.2				
NR(4 Ge)						4.0	1.3	0.2	0.2	
NR(5 Ge)							0.2	2.6	1.4	0.3
NR(6 Ge)									0.1	4.0

TABLE IV. Average number (expressed as a percentage) of Ge and Se atoms involved in threefold and fourfold coordinations (for Ge) and onefold, twofold, and threefold coordinations (for Se). We compare the values obtained in the present work with those obtained through a MD scheme based on a non-self-consistent DFT electronic structure scheme (Ref. 16) and through an ECMR method (Ref. 21). The symbol A=Ge,Se indicates that the identity of the atoms bonded to Ge or Se is not specified. We also compare (in percentages) the number of Ge atoms forming edge-sharing connections, N_{Ge}(ES), the number of Ge atoms forming corner-sharing connections, N_{Ge}(CS), the number of Ge atoms involved in homopolar bonds, $N_{Ge\text{-}Ge}$, and the number of Se atoms involved in homopolar bonds, $N_{Se\text{-}Se}$. Experimental values are taken from Ref. 10.

	This work	MD	ECMR	Expt.
Ge				
GeA_3 (A=Ge,Se)	8±1	15	19	
Ge-$GeSe_3$	5±2	25	6	
$GeSe_4$	70±4	61	75	
Se				
SeA_2 (A=Ge,Se)	92±3	70	72	
SeA_3 (A=Ge,Se)	4±1	20	18	
SeA (A=Ge,Se)	4±1	10	10	
N_{Ge}(ES)	45±4	47	38	34
N_{Ge}(CS)	50±6	28	45	41
$N_{Ge\text{-}Ge}$	5±2	25	17	25
$N_{Se\text{-}Se}$	24±2	25	30	20

In Table II, the calculated concentrations of Ge atoms in edge-sharing [N_{Ge}(ES)] and corner-sharing [N_{Ge}(CS)] configurations are compared to experimental estimates.[10] The percentage number of Ge and Se atoms involved in homopolar bonds are also given. To obtain N_{Ge}(CS), we adopted the proposal of Ref. 10, i.e., $N_{Ge}(CS)=1-N_{Ge}^{th(a)}(ES)-N_{Ge\text{-}Ge}$, which holds in the absence of extended chains.[10] The calculated concentrations of Ge atoms in corner-sharing and edge-sharing configurations are slightly larger than those derived from neutron diffraction data [(50±6)% vs 41%] and [(45±4)% vs 34%].

E. Comparison to previous DFT-based approaches

In Table IV our results for the coordination numbers are compared to those obtained by the group of Drabold.[16,21] Two sets of results are considered. The first set corresponds to a molecular dynamics (MD) approach based on a non-self-consistent electronic structure scheme, in which the local density approximation of DFT was used in combination with a minimal basis set. The structural model was cooled down to a temperature of 300 K over a period of 4 ps and finally quenched to T=0 K.[16] The final structure consisted of 144 Se atoms and 72 Ge atoms in a periodically repeated cubic cell. The second set corresponds to the combination of the former molecular dynamics scheme with a reverse Monte Carlo method.[21] In Ref. 21, this approach was termed experimentally constrained molecular relaxation (ECMR) and was intended to provide a generation procedure that improved upon quench simulations from melt. Herafter, we shall refer to these two schemes as MD and ECMR, respectively.

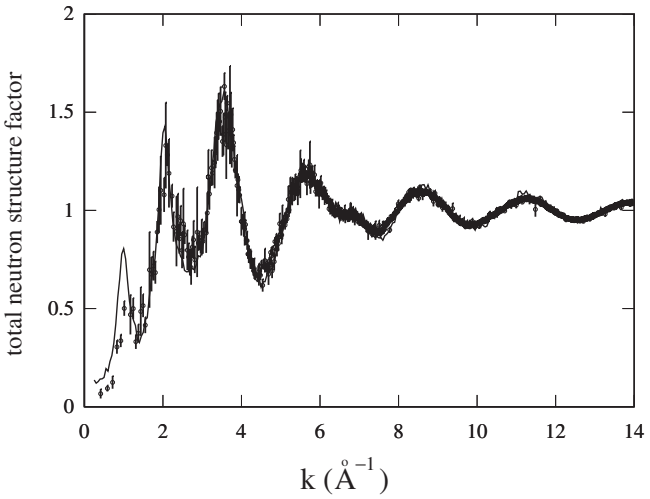

FIG. 5. Total neutron structure factor of amorphous $GeSe_2$: present simulation (circles with error bars) compared to experimental data (solid line, Ref. 42). We used scattering lengths of b_{Ge}=8.189 and b_{Se}=7.97 fm (Ref. 10).

The most notable feature of the MD approach is the large deviation from chemical order, expressed by 61% of the Ge atoms and 70% of the Se atoms being fourfold and twofold coordinated, respectively. Applied to the liquid the same scheme gave very close values (58% for Ge and 62% for Se, see Ref. 17), suggesting that the glassy structure underwent only a limited relaxation. The ECMR approach restored some chemical order as evidence by the Ge coordination, but the amount of Se atoms miscoordinated remained as high as 28%. ECMR also improved upon MD the number of Ge atoms in edge-sharing and corner-sharing configurations, leading to good agreement with experiment [N_{Ge}^{ECMR}(ES)=38% vs N_{Ge}^{expt}(ES)=34%, N_{Ge}^{ECMR}(CS)=45% vs N_{Ge}^{expt}(ES)=41%]. This occurs at the expense of the number of Ge atoms involved in homopolar bonds [$N_{Ge\text{-}Ge}$=25% in MD, $N_{Ge\text{-}Ge}$=17% in ECMR, to be compared to the experimental estimate of 25% (Ref. 10)]. It would be interesting to ascertain whether these values would change for longer relaxation runs, comparable to those in the present work (cf. Sec. II).

IV. RECIPROCAL SPACE PROPERTIES

A. Total neutron structure factor and Faber–Ziman partial structure factors

In Fig. 5, the calculated total neutron structure factor $S_T(k)$ is compared to its experimental counterpart.[42] Two behaviors are clearly distinguishable. For $k \geq 2$ Å^{-1}, peak positions and intensities are well reproduced within statistical errors. On the other hand, for $k<2$ Å^{-1}, the FSDP height is underestimated and the shape of $S_T(k)$ differs from the experimental pattern, with the absence of a clear minimum between the first two peaks. The origin of this disagreement

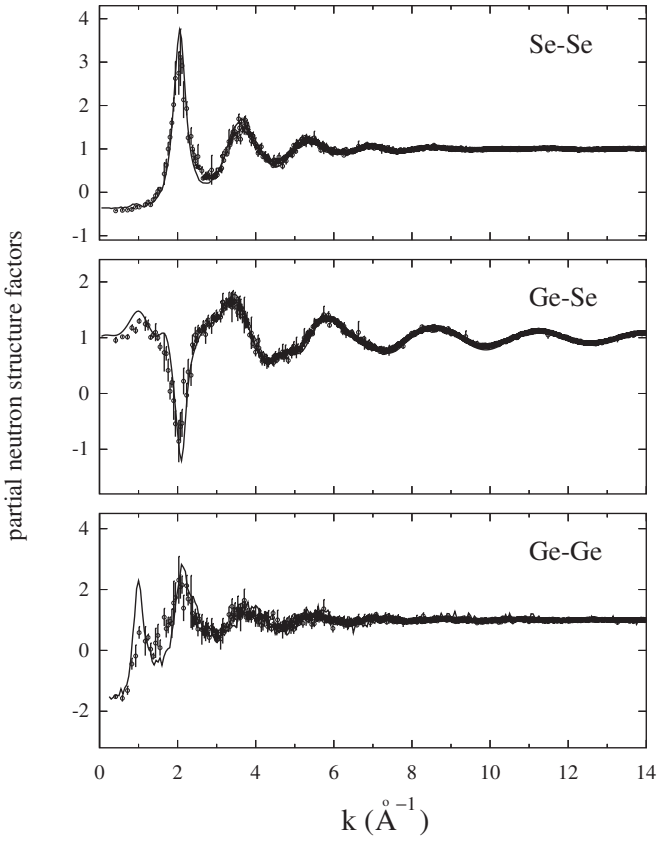

FIG. 6. Faber–Ziman partial structure factors of amorphous $GeSe_2$: present simulation (circles with error bars) compared to experimental data (solid line, Ref. 9).

can be traced back to the Faber–Ziman partial structure factors $S_{SeSe}(k)$, $S_{GeSe}(k)$, and $S_{GeGe}(k)$, as shown in Fig. 6. In the case of $S_{SeSe}(k)$ and $S_{GeSe}(k)$, theory and experiments agree over the entire k range, with a remarkable agreement for the position of the peaks, their intensities and the sequence of maxima and minima. The only notable exception is found in $S_{GeSe}(k)$, for which the FSDP height is slightly underestimated. The remarkable performance of theory in reproducing the $S_{SeSe}(k)$ and $S_{GeSe}(k)$ structure factors is consistent with the very good agreement between the corresponding experimental and theoretical pair correlation functions.

The comparison between theory and experiment is less satisfactory in the case of $S_{GeGe}(k)$. Although the FSDP position is well reproduced, $S^{th}_{GeGe}(k)$ substantially differs from $S^{exp}_{GeGe}(k)$ in the region $k<3$ Å^{-1} (see Fig. 6). Along with a reduction of the FSDP intensity in $S^{th}_{GeGe}(k)$, one notices a broadening toward lower k values of the second peak and the absence of a pronounced minimum between the first two peaks. $S^{th}_{GeGe}(k)$ is less structured than $S^{exp}_{GeGe}(k)$, as expected in view of the flattened shape of $g^{th}_{GeGe}(r)$. Based on these results, the underestimation of the FSDP height in the total neutron structure factor is due predominantly to the $S_{GeGe}(k)$ contribution, lower than in the experiment. We recall that in the case of liquid $GeSe_2$ the underestimation of the FSDP in $S_{GeGe}(k)$ was compensated by an overestimation in $S_{GeSe}(k)$.[26,28] This gave excellent agreement between theory and experiment over the full k range for the total neutron structure factor.

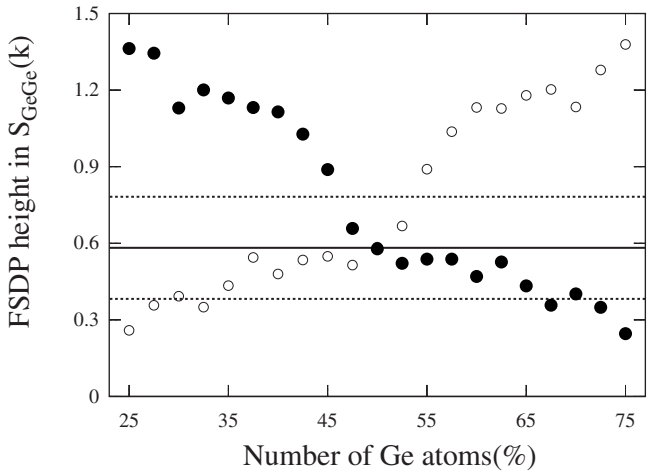

FIG. 7. Height of the FSDP in $S_{GeGe}(k)$ as a function of the number of Ge atoms belonging to fourfold rings, Ge(1)+Ge(2) (open circles), and not belonging to fourfold rings, Ge(0) (filled circles). A continous line is drawn at the average value of 0.58, together with two dotted lines indicating the extent of the error bar.

Ordering on a range extending up to 60 Å has been recently discovered for several network forming glasses, including a-$GeSe_2$.[43] The present approach is in principle not suited for calculating real space properties beyond the repeat length of the cubic simulation cell. Extended order can be described in terms of the position of the second peak k_{sp} and of its width Δk_{sp} in the partial structure factors.[38,43] Surprisingly, these two features are rather well reproduced by our calculations for $S_{SeSe}(k)$ and $S_{GeSe}(k)$. In the case of $S_{GeGe}(k)$, the position of the second peak in $S^{th}_{GeGe}(k)$ and its width differ from the experiment by only 2% and 15%, respectively. It is presently not clear whether the level of agreement found for k_{sp} and Δk_{sp} is fortuitous or whether this implies that the infinitely periodic model is able to capture the extended ordering in a-$GeSe_2$.

It is of interest to seek correlations between the height of the FSDP and specific structural features. Hereafter, we shall focus on the height of the FSDP in $S_{GeGe}(k)$ (FSDP-h) and on the number of Ge(0), Ge(1) and Ge(2) atoms. For this purpose, the instantaneous values of these properties were recorded over the six trajectories. Then, we calculated, for each given amount of Ge(0) and Ge(1)+Ge(2), the corresponding average value of FSDP-h. In Fig. 7, the results are displayed together with the average value and error bar (0.58 ± 0.20) for $S_{GeGe}(k)$ at the FSDP location. We recall that the experimental FSDP height in $S_{GeGe}(k)$ is equal to 2.29. The patterns of Ge(0) and Ge(1)+Ge(2) are symmetrical by construction and indicate an increase of FSDP-h with increasing number of edge-sharing connections. However, extrapolation of FSDP-h toward values beyond 1.5 leads to an unphysically high population of edge-sharing Ge atoms, in disagreement with the experimental result. Therefore, as far as the FSDP height of $S_{GeGe}(k)$ is concerned, the origin of the difference between theory and experiment cannot simply be ascribed to a reduced number of Ge atoms in edge-sharing tetrahedra.

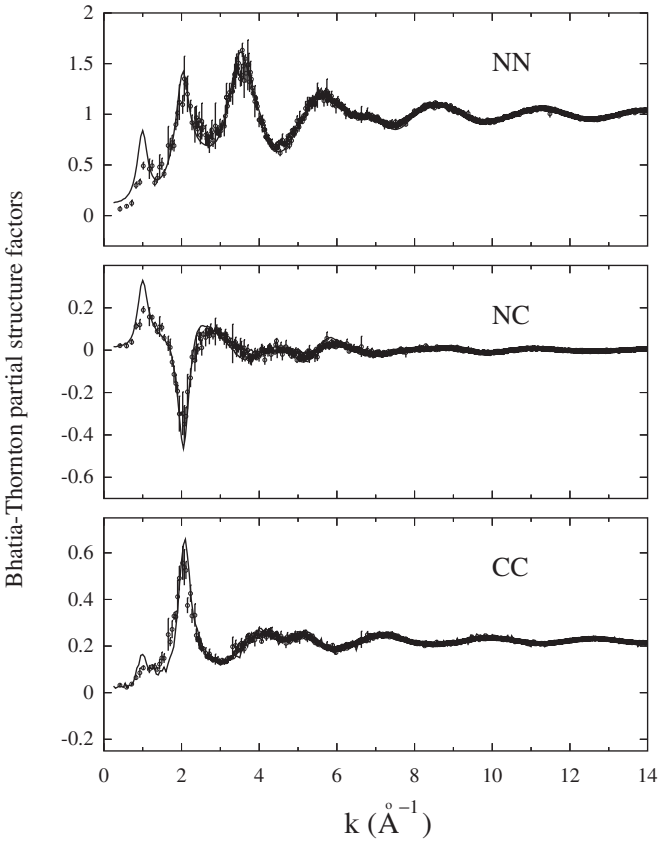

FIG. 8. Bhatia–Thornton partial structure factors of amorphous $GeSe_2$: present simulation (circles with error bars) compared to experimental data (solid line, Ref. 9).

B. Bhatia–Thornton partial structure factors

In Fig. 8, we focus on the Bhatia–Thornton partial structure factors $S_{NN}(k)$ (number–number), $S_{NC}(k)$ (number–concentration), and $S_{CC}(k)$ (concentration-concentration).[44] These can be obtained by linear combinations of the Faber–Ziman structure factors.[45] In terms of the Bhatia–Thornton structure factors, the total neutron structure factor $S_T(k)$ reads

$$S_T(k) = S_{NN}(k) + A[S_{CC}(k)/c_{Ge}c_{Se} - 1] + BS_{NC}(k), \quad (1)$$

where $A = c_{Ge}c_{Se}\Delta b^2/\langle b\rangle^2$, $B = 2\Delta b/\langle b\rangle$, $\Delta b = b_{Ge} - b_{Se}$, $\langle b\rangle = c_{Ge}b_{Ge} + c_{Se}b_{Se}$, and c_α and b_α denoting the atomic fraction and the coherent scattering length of the chemical species α ($b_{Ge} = 8.185$ fm, $b_{Se} = 7.97$ fm).[10] This leads to coefficients A and B equal to 1.6×10^{-4} and 0.053, respectively. Due to the close values of the scattering lengths of Ge and Se, and the limited range of variation of $S_{NC}(k)$ and $S_{CC}(k)$ ($|S_{NC}(k)| < 0.4$, $S_{CC}(k) < 0.8$, see Fig. 8), $S_{NN}(k)$ turns out to be a very good approximation for $S_T(k)$, i.e., $|S_T(k) - S_{NN}(k)| < 0.025$. Therefore, the considerations developed for $S_T(k)$ and based on Fig. 5 equally apply well to the behavior of $S_{NN}(k)$, as shown in Fig. 8.

The $S_{NC}(k)$ partial structure factor is given by

$$S_{NC}(k) = c_{Ge}c_{Se}\{c_{Ge}[S_{GeGe}(k) - S_{GeSe}(k)] - c_{Se}[S_{SeSe}(k) - S_{GeSe}(k)]\}. \quad (2)$$

In the FSDP region of $S_{NC}(k)$, the positive contribution is due to the products $c_{Ge}S_{GeGe}(k)$ and $c_{Se}S_{GeSe}(k)$. Both of them are larger in the experimental Faber–Ziman structure factor. As to the main negative peak of $S_{NC}(k)$ at $k \sim 2$ Å^{-1}, the predominant contribution arises from the very intense main peak in $S_{SeSe}(k)$, a feature very well reproduced by our calculations.

Special attention has been devoted in the literature to the Bhatia–Thornton concentration-concentration partial structure factor $S_{CC}(k)$, defined as

$$S_{CC}(k) = c_{Ge}c_{Se}(1 + c_{Ge}c_{Se}\{[S_{GeGe}(k) - S_{GeSe}(k)] + [S_{SeSe}(k) - S_{GeSe}(k)]\}). \quad (3)$$

This quantity expresses the overall sensitivity to chemical disorder and accounts for contributions due to the chemical environment of each atom.[46] Therefore, each peak is representative of fluctuations of concentration associated to the specific value of k. Early first-principles molecular dynamics of liquid $GeSe_2$ did not show any FSDP in the $S_{CC}(k)$, in disagreement with experiments.[26] To understand the origin of this behavior, the intensities of the FSDP in the $S_{CC}(k)$ have been compared for a series of liquid and glasses.[47] We showed that the FSDP in $S_{CC}(k)$ occurs for moderate departures from chemical order but vanishes either for high levels of structural disorder or when the chemical order is essentially perfect.[47] In a further analysis, carried out on liquid $GeSe_2$, we have found that a sequence of connected fourfold rings can be taken as the structural fingerprint for the presence of a FSDP in $S_{CC}(k)$.[48] Similar conclusions can be extracted from a study on the liquids of $GeSe_2$ and $ZnCl_2$ based on classical molecular dynamics and a polarizable ion model.[49]

Our calculated $S_{CC}(k)$ agrees very well with its experimental counterpart in the range $k \geqslant 2$ Å^{-1}. The height and intensity of the main peak are accurately reproduced in the simulation. At lower k values, the main peak is slightly larger and the FSDP feature observed in the experiment takes the form of a shoulder extending over the interval $1 < k < 1.7$ Å^{-1}. The underestimation of the FSDP height in $S_{CC}(k)$ can be attributed to the difference between theory and experiment in $S_{GeGe}(k)$. The presence of the FSDP in $S_{CC}(k)$ is consistent with the previously identified relationship between a small departure from chemical order and the appearance of the FSDP.[47] Indeed, a FSDP in $S_{CC}(k)$ appears in the case of amorphous $SiSe_2$ and liquid $GeSe_4$. These systems exhibit limited departures from chemical order due to both homopolar bonds and miscoordinations.[50,51] Our model is characterized by a sizeable number of miscoordinations (GeSe, $GeSe_2$, $GeSe_3$, $GeGeSe_3$, and $GeSe_4$ units for Ge and SeGe, $SeSe_2$, SeGe, $SeGe_2$, and $SeGe_3$ units for Se), but by very few Ge atoms forming homopolar bonds, $N_{Ge\text{-}Ge}$. Therefore, the intensity of the FSDP in the $S_{CC}(k)$ partial structure factor of a-$GeSe_2$ is expected to increase further in an improved model featuring a moderately larger number of Ge-Ge homopolar bonds.

V. CONCLUSIONS

Disordered $GeSe_2$ systems are materials combining the predominant presence of tetrahedra and a nonnegligible concentration of homopolar bonds and miscoordinations. This behavior results from the subtle interplay between the ionic and the covalent character of the bonding, due to the close electronegativities of Ge and Se. Therefore, a first-principles determination of structural properties is best suited to ensure a realistic comparison with experiments. In recent years, we have studied in detail the short and intermediate range structure of liquid $GeSe_2$ by using a first-principles molecular dynamics approach.[26,27] The very good agreement achieved with neutron diffraction data has made the application of the same approach to the case of amorphous $GeSe_2$ worth pursuing. To this end, several temporal trajectories have been produced via quenches from independent configurations of the liquid. The reduction of the concentration of structural defects that has followed the cooling process shows that the very high cooling rates do not prevent the system from adjusting to a change of thermal conditions. Pair correlation functions exhibit very satisfactory agreement with the experiment in the case of Ge-Se and Se-Se correlations. The number of Se-Se homopolar bonds and the Ge-Se coordination numbers are only moderately larger than in the experiments. The reliability of our approach worsens in the case of Ge-Ge correlations, confirming a trend previously observed in the case of liquid $GeSe_2$. Two shortcomings are worth pointing out. First, the overall profile of $g^{\mathrm{th}}_{\mathrm{GeGe}}(r)$ when compared to $g^{\mathrm{exp}}_{\mathrm{GeGe}}(r)$ is much less structured, lacking a well defined minimum between the first ($r<4.5$ Å) and the second (4.5 Å$<r<8$ Å) shell of neighbors. Second, the number of homopolar Ge-Ge bonds is underestimated, indicating that most of the Ge-Ge short distances found in the liquid do not survive the cooling and relaxation process. In a previous paper, we demonstrated that the use of the generalized gradient approximation improved the structural description upon that achieved with the local density approximation due to a more accurate treatment of the ionic character of bonding.[27] The residual differences between theory and experiments observed for both amorphous and liquid $GeSe_2$ then suggest that the generalized gradient approximation adopted in our studies yet provides an insufficient account of the ionic character of the bonding.[28] It remains to be understood whether this rationale could also account for the low concentration of homopolar Ge-Ge bonds.

Amorphous $GeSe_2$ is more chemically ordered than the corresponding liquid, with as much as $(75\pm6)\%$ and $(93\pm6)\%$ of Ge and Se atoms fourfold and twofold coordinated, respectively. Also, the variety of different bonding configurations is smaller than in the liquid, encompassing only GeSe, $GeSe_2$, $GeSe_3$, $GeGeSe_3$, and $GeSe_4$ units for Ge and SeGe, $SeSe_2$, SeGe, $SeGe_2$, and $SeGe_3$ units for Se. In comparison to experiments, it appears that Ge atoms do prefer to deviate from chemical order by forming groups other than $GeSe_4$ rather than forming Ge-Ge dimers or chains. Restoring chemical order upon cooling also has the effect of favoring the formation of even-membered rings (mostly four and six membered) with an equal number of Ge and Se atoms. In this respect, it is worth mentioning the principal result from a recent investigation of the vibrational properties.[24] On the basis of comparisons between calculated and measured infrared and Raman spectra, the occurrence of a strong chemical order in a-$GeSe_2$ could be inferred.[24]

An important issue in the description of a disordered network such as amorphous $GeSe_2$ is the amount of edge-sharing and corner-sharing connections. In our model, close concentrations are found for Ge atoms occurring in edge-sharing and corner-sharing configurations: $N_{\mathrm{Ge}}(\mathrm{ES})=(45\pm4)\%$ and $N_{\mathrm{Ge}}(\mathrm{CS})=(50\pm6)\%$. The remaining Ge atoms $[(5\pm2)\%]$ are involved in homopolar bonds.

Overall, total and partial structure factors reproduce the experimental peak positions and intensities for k values larger than 2 Å^{-1}. For smaller values, representative of intermediate range order, a substantial reduction in the height of the FSDP is observed for $S_{\mathrm{GeGe}}(k)$, resulting in a similar behavior for the total neutron structure factor. These differences between theory and experiment result from real-space correlations at distances beyond $r\sim4.5$ Å.[52] Based on the corresponding $g_{\mathrm{GeGe}}(r)$ pair correlation function, it indeed appears that the theoretical description lacks a distinct minimum between the first ($r<4.5$ Å) and the second (4.5 Å$<r<8$ Å) shell of Ge neighbors. We found a discernible feature at the FSDP location in the $S_{\mathrm{CC}}(k)$ structure factor. In agreement with previous results obtained on several disordered network-forming systems, this finding is consistent with the moderate departure from chemical order we observed in our model a-$GeSe_2$.

Our study provides an atomic-scale description of amorphous $GeSe_2$ of unprecedented quality. However, the still unsatisfactory behavior of Ge-Ge correlations is a motivation for further improving our theoretical scheme. Two strategies are worth to be outlined. Calculations with larger simulation cells will allow us to ascertain whether subtle size effects may alter the arrangement of Ge atoms within the network. Especially for Ge, this issue might play a role in view of the limited number of these atoms (40) in the present calculations. We provided arguments supporting the adequacy of our computational cells to describe intermediate range order.[28] Nevertheless, calculations involving about 150 Ge atoms (for a total close to 500) will be instrumental to clarify this issue. A further approach consists in employing different families of exchange-correlation functionals, in search of a better account of the ionic character of the system. As already observed in the case of liquid $GeSe_2$, this idea is consistent with our findings of excessively large Ge-Ge bond lengths, which are characteristic of metallic liquid Ge.

ACKNOWLEDGMENTS

We thank P. S. Salmon for stimulating exchanges. The calculations were performed on the NEC-SX5 of the Swiss Center for Scientific Computing (CSCS) and on the NEC-SX5 of the IDRIS computer center of CNRS (France).

[1] S. C. Moss and D. L. Price, in *Physics of Disordered Materials*, edited by D. Adler, H. Fritzsche and S. R. Ovshinsky (Plenum, New York, 1985), p. 77.
[2] P. Boolchand and W. J. Bresser, Philos. Mag. B **80**, 1757 (2000).
[3] W. H. Zachariasen, J. Am. Chem. Soc. **54**, 3841 (1932).
[4] *The Physics and Technology of Amorphous* SiO_2, edited by R. A. B. Devine (Plenum, New York, 1988).
[5] J. Sarnthein, A. Pasquarello, and R. Car, Phys. Rev. Lett. **74**, 4682 (1995).
[6] J. Sarnthein, A. Pasquarello, and R. Car, Phys. Rev. B **52**, 12690 (1995).
[7] W. J. Bresser, P. Boolchand, P. Suranyi, and J. P. de Neufville, Phys. Rev. Lett. **46**, 1689 (1981).
[8] P. Boolchand, J. Grothaus, W. J. Bresser, and P. Suranyi, Phys. Rev. B **25**, 2975 (1982).
[9] I. Petri, P. S. Salmon, and H. E. Fischer, Phys. Rev. Lett. **84**, 2413 (2000).
[10] I. Petri and P. S. Salmon, J. Phys.: Condens. Matter **15**, S1509 (2003).
[11] P. Tronc, M. Bensoussan, A. Brenac, and C. Sebenne, Phys. Rev. B **8**, 5947 (1973).
[12] A. Fischer-Colbrie and P. H. Fuoss, J. Non-Cryst. Solids **126**, 1 (1990).
[13] S. Sugai, Phys. Rev. B **35**, 1345 (1987).
[14] S. R. Elliott, Nature (London) **354**, 445 (1991).
[15] P. Vashishta, R. K. Kalia, G. A. Antonio, and I. Ebbsjö, Phys. Rev. Lett. **62**, 1651 (1989); P. Vashishta, R. K. Kalia, J. P. Rino, and I. Ebbsjö, Phys. Rev. B **41**, 12197 (1990); H. Iyetomi, P. Vashishta, and R. K. Kalia, *ibid.* **43**, 1726 (1991).
[16] M. Cobb, D. A. Drabold, and R. L. Cappelletti, Phys. Rev. B **54**, 12162 (1996).
[17] M. Cobb and D. A. Drabold, Phys. Rev. B **56**, 3054 (1997).
[18] X. Zhang and D. A. Drabold, Phys. Rev. B **62**, 15695 (2000).
[19] M. Durandurdu and D. A. Drabold, Phys. Rev. B **65**, 104208 (2002).
[20] D. N. Tafen and D. A. Drabold, Phys. Rev. B **68**, 165208 (2003).
[21] P. Biswas, D. N. Tafen, and D. A. Drabold, Phys. Rev. B **71**, 054204 (2005).
[22] D. N. Tafen and D. A. Drabold, Phys. Rev. B **71**, 054206 (2005).
[23] J. C. Mauro and A. K. Varshneya, J. Am. Ceram. Soc. **89**, 2323 (2006).
[24] L. Giacomazzi, C. Massobrio, and A. Pasquarello, Phys. Rev. B **75**, 174207 (2007).
[25] I. Petri and P. S. Salmon, Phys. Chem. Glasses **43C**, 185 (2002).
[26] C. Massobrio, A. Pasquarello, and R. Car, Phys. Rev. Lett. **80**, 2342 (1998).
[27] C. Massobrio, A. Pasquarello, and R. Car, J. Am. Chem. Soc. **121**, 2943 (1999).
[28] C. Massobrio, A. Pasquarello, and R. Car, Phys. Rev. B **64**, 144205 (2001).
[29] C. Massobrio, F. H. M. Van Roon, A. Pasquarello, and S. W. de Leeuw, J. Phys.: Condens. Matter **12**, L697 (2000).
[30] R. Car and M. Parrinello, Phys. Rev. Lett. **55**, 2471 (1985).
[31] K. Laasonen, A. Pasquarello, R. Car, C. Lee, and D. Vanderbilt, Phys. Rev. B **47**, 10142 (1993).
[32] J. P. Perdew, J. A. Chevary, S. H. Vosko, K. A. Jackson, M. R. Pederson, D. J. Singh, and C. Fiolhais, Phys. Rev. B **46**, 6671 (1992).
[33] A. Dal Corso, A. Pasquarello, A. Baldereschi, and R. Car, Phys. Rev. B **53**, 1180 (1996).
[34] C. Massobrio and A. Pasquarello, J. Chem. Phys. **114**, 7976 (2001).
[35] S. Nosé, Mol. Phys. **52**, 255 (1984); W. G. Hoover, Phys. Rev. A **31**, 1695 (1985).
[36] P. E. Blöchl and M. Parrinello, Phys. Rev. B **45**, 9413 (1992).
[37] F. H. M. Van Roon, C. Massobrio, E. de Wolf, and S. W. de Leeuw, J. Chem. Phys. **113**, 5425 (2000).
[38] P. S. Salmon, J. Phys.: Condens. Matter **19**, 455208 (2007).
[39] S. V. King, Nature (London) **213**, 1112 (1967).
[40] D. S. Franzblau, Phys. Rev. B **44**, 4925 (1991).
[41] V. Rosato, M. Celino, G. Benedek, and S. Gaito, Phys. Rev. B **60**, 16928 (1999).
[42] S. Susman, K. J. Volin, D. G. Montague, and D. L. Price, J. Non-Cryst. Solids **125**, 168 (1990).
[43] P. S. Salmon, R. A. Martin, P. E. Mason, and G. J. Cuello, Nature (London) **435**, 75 (2005).
[44] A. Bhatia and D. Thornton, Phys. Rev. B **2**, 3004 (1970).
[45] The relationship between the three sets of partial structure factors commonly used (Faber–Ziman, Ashcroft–Langreth, and Bhatia–Thornton) can be found in Y. Waseda, *The Structure of Non-Crystalline Materials* (McGraw-Hill, New York, 1980).
[46] P. S. Salmon, Proc. R. Soc. London, Ser. A **437**, 591 (1992).
[47] C. Massobrio, M. Celino, and A. Pasquarello, Phys. Rev. B **70**, 174202 (2004).
[48] C. Massobrio and A. Pasquarello, Phys. Rev. B **75**, 014206 (2007).
[49] B. K. Sharma and M. Wilson, Phys. Rev. B **73**, 060201(R) (2006).
[50] M. Celino and C. Massobrio, Phys. Rev. Lett. **90**, 125502 (2003).
[51] M. J. Haye, C. Massobrio, A. Pasquarello, A. De Vita, S. W. de Leeuw, and R. Car, Phys. Rev. B **58**, R14661 (1998).
[52] P. Vashishta, R. K. Kalia, and I. Ebbsjö, Phys. Rev. B **39**, 6034 (1989).